Automatic Detection and Picking of Local and Regional S-Waves

Nasim Karamzadeh[1], Gholam Javan-Doloei[2*], Peter Voss[3], and Ali M. Reza[4]

1. Ph.D. Student, Seismology Research Center, International Institute of Earthquake Engineering and Seismology (IIEES), Iran
2. Assistant Professor, Seismology Research Center, International Institute of Earthquake Engineering and Seismology (IIEES), Iran,
* Corresponding Author; e-mail: javandoloei@iiees.ac.ir
3. Ph.D., Geological Survey of Denmark and Greenland (GEUS), Oster Voldgade 10, DK-1350 Copenhagen K, Denmark
4. Professor, University of Wisconsin-Milwaukee, Electrical Engineering and Computer Science Milwaukee, Wisconsin, United States

Received: 06/06/2012
Accepted: 03/12/2012

ABSTRACT

In this paper, automatic detection and picking of the S-wave, in the problem of passive seismic monitoring has been studied, and a method is proposed for detecting S-phase onset time based on the eigenvalue analysis. By calculating eigenvalues of the time domain covariance matrix of the earthquake record, a characteristic function is defined, in which applying an adaptively determined threshold value, the S-phase onset time is picked. The proposed method is capable of successful determining S-phase onset time in local and near regional seismograms. Motivation towards this research has been the growing number of operating seismic stations in Iranian Broadband Network (BIN) and the necessity of providing earthquake parameters information fast and precisely. In addition, a doing well S-phase picking algorithm can be used to increase the number of determined S-phases in databases in which tomography studies are carried on. We tested the proposed method on 185 earthquakes recorded in the BIN, and evaluated the performance of the algorithm. We also examined the other algorithm of S-phase detection based on Autoregressive (AR) modeling of the seismograms on the same data, and compare the output of two algorithms. This comparison implies that the results of the proposed method are better than the AR based algorithm on our database.

Keywords:
Automatic phase picking; Covariance matrix; Eigenvalue; S-phase picker

1. Introduction

Automatic earthquake signal phase picking is of great importance in earthquake data processing. Modern digital seismic networks, which are operating continuously all over the world, produce huge data. The manual processing of the increasing amount of such data is very time consuming and requires considerable work force. Therefore, from early days of digital seismology, a considerable effort has been done in order to automate different steps of earthquake signal processing. Consequently, nowadays, real-time automatic procedures that include both data acquisition and data processing modules are commonly used in every earthquake data processing centers, e.g. the Earthworm System [1], which is supported by the USGS, is operating in most US seismic networks. The event and phase detector algorithms used in real-time procedures are usually based on the STA (short term average) / LTA (long term average) algorithm (e.g. [2-3]). The fundamental of this method is to compute the average amplitude of the signal, or an improved version of it, in two running time window, one with a short duration, and the other with longer duration. The phase detection is then achieved when the STA/LTA becomes larger than a

predefined threshold level. The STA/LTA based algorithms may be sufficient for rapid earthquake location estimation. However, for precise location of the earthquakes and further seismological studies, such as tomographic studies, more accurate phase picking algorithms are needed.

Seismic phases are detectable by exploring the variation of local properties of the seismograms, such as the frequency content, amplitude, statistical properties and polarization. In order to detect seismic phases using automatic algorithms, such variations should be investigated on the seismogram or on a characteristic function (CF). The concept of the CF is first introduced by Allen [2], and is a time series that efficiently characterizes the seismogram, and responds to the desired changes as rapidly as possible while preferably enhances them. The performance of a phase picker algorithm relies strongly on the CF, so it should be defined very carefully depending on the properties of the analyzing seismograms and the desired seismic phase. The absolute amplitude, power, polarization indicators and the envelope function of the seismogram are usually selected as a CF both for P- and S-phase onset detection [2-8]. While the automatic methods of P-phase detection picking are more likely to perform successfully, the scenario for S-phase is usually more complicated. The S-phase detection and phase picking, which we consider in this paper, needs to be done against the background of the P-phase coda. The S-phase commencement on the seismogram is often emergent and buried in the P-phase coda; though at very short distances, the S-phase onset can be impulsive and have high amplitude relative to the P-phase coda. Furthermore, converted S-to-P or P-to-S phases at a sediment-bedrock interface may be misinterpreted as the first S-phase onset time [9]. For example, Sp precursor, S-to-P conversion, appears on the seismogram ahead of S by a time proportional to the depth of the interface and the V_p/V_s ratio in the crust [10]. Hence, even manual S-phase picking is often uncertain for many seismogram signals. Accordingly, S-phase onset time will not be reported for many seismograms, e.g., during 2008, the total number of P (Pn and Pg) and S (Sg and Sn) phases reported by the ISC bulletin were about 273000 and 118000 phases, respectively [11]. However, S-wave arrival time is very important to have a robust and reliable earthquake location. At least one S-phase reading is required at a station within approximately 1.4 focal depth's distance from the source to derive a focal depth that is accurate to within approximately ±1.5 km [12]. Moreover, determination of shear wave velocity is a key parameter to calculate Poisson's ratio that is important in petrological aspects [13-14]. Therefore, we need to have S-phase onset time in dataset in which seismic tomographic studies are done. The problem we are dealing with in this paper is to detect the S-phase automatically and to pick its arrival time, once the P-phase arrival time is already available with high precision via manual processing or automatic procedure (e.g. [15]), and the preliminary location of the seismic event is also available. We need the event location to be known, in order to discard false detection of other secondary phases instead of the first arriving S-phases. This task simply is done by comparing a rough estimation of receiver-to-source distance, having the S-P time, with which existed in the catalogue.

Automatic S-phase picking algorithms usually rely on inherent difference of P- and S-phase characteristics as described thoroughly in [16-17]. The S-phase is always delayed as compared to the P-phase arrival time at the station, and the amount of the corresponding delay depends on the epicentral distance and the earth velocity model. We have benefitted from this property in our S-phase detection method. Theoretically, first emerging P-phase particle motion aligns in the direction of the propagation path, while S-phase oscillates in a plan perpendicular to the wave propagation direction, called the S-plane. Any S wave signal consists of SH and SV components, which may or may not be well-correlated at zero lag. Within the solid earth, the particle motion of these components will be linearly polarized and perpendicular to the ray direction. Because of reflections at the earth surface, this property can not be easily observed on the recorded seismogram unless the wave arrives close to the vertical direction. However, if the SV wave arrives at the surface post-critically, then both the horizontal and vertical components are shifted in phase [18], then the registered signal is no longer linearly polarized. Discriminating between P- and S-wave groups

can be done using so called polarization analysis, both in time and frequency domains, which traditionally known as the essential tool for identifying the presence of S-phase on the earthquake record. Traditional approaches to the polarization analysis are very well known in seismology and have been discussed in various papers (e.g. [6, 17, 18, 19, 20]). For large epicentral distances, where P-phase energy dominantly appears in the vertical component and S-phase appears in the horizontal components, the S-phase detector can be defined based on the propagation of energy in the horizontal plane based on polarization analysis. In this case, using STA/LTA detection procedure, S-phase or other secondary phases can be detected [21]. For example, Earle and Shearer [5] have applied an STA/LTA detector on the envelope function of the seismograms to derive travel time curves using automatically picked phases. Combination of the polarization analysis and the wavelet transform has been proposed in many studies (e.g. [6, 22, 23]). In [23], this approach has been verified using regional seismograms recorded more than 900 km far away epicenter. Autoregressive (AR) modeling of the earthquake record has been investigated for estimation of P- and S-phase onset time, and online system of earthquake location [22, 24, 25]. It has been observed in [24] and [25] that although for P-phase onset determination based on the AR modeling, using single vertical component is sufficient, for accurate estimation of S-phase, using two or three components, seismic data is a better choice. In this case, every component can be processed separately and the earlier time can be considered as the onset time. In addition, AR models derived from every component can be analyzed jointly to determine S-phase onset time [24]. Kuperchoch [26] used the AR forward prediction of S-wave by applying an AR model to both horizontal components. Afterward, comparing the predicted waveforms with the incoming ones, a prediction error is determined which provides a CF, to which S-phase detection is done through an iterative procedure.

In the current study, we aim to introduce a method to determine S-phase onset time automatically for local (less than 100 km) and near regional seismograms (100-400 km). The method is based on the eigenvalue analysis of the time domain 3D covariance matrix and Akaike's Information Criteria (AIC) [27]. However, a 2D covariance matrix based on horizontal components is also applicable. Motivation towards this research has been growing the number of operating seismic stations in Iranian Broadband Network (BIN) and necessity of providing fast and precise information of the earthquake parameters. Implementing an automatic detection procedure on BIN in combination of manual processing of data may lead to fast processing and dissemination of the earthquake data.

2. Autoregressive Modeling and AIC Criteria

Autoregressive (AR) modeling has been used in many automatic phase picking procedures to obtain accurate estimation of P- and S-phase onset time [22, 24, 25, 26, 28, 29]. A brief introduction to the AR modeling and its rule in seismic phase picking is presented in what follows.

Assume a segment of seismogram that includes a seismic phase onset time whose precise time is unknown; the rule of the AR modeling is to determine the precise phase onset time, in other words, an optimum division point in this segment. This process involves calculating the AR model of the seismogram segment, x_n, $n = 1, ..., N$ where N is the length of the segment, in two intervals; one, $i = 1$, is selected before the start of the phase and consists of seismic background noise only, and the other, $i = 2$, is selected after phase arrival time, which includes seismic background noise as well as seismic signal. It is required that x_n includes a sufficiently long segment before and after the real onset time to make an effective AR model fit for both intervals separately. It has been assumed that both intervals can be modeled as stationary processes with uncorrelated Gaussian noise. In both intervals, $i = 1$, 2, the data can be fitted to an autoregressive model of the fixed order M, but independent coefficients, $a_m^i = m = 1,...,M$:

$$x_n = \sum_{m=1}^{M} a_m^i x_{n-m} + \varepsilon_n^i \tag{1}$$

with $n = 1, ..., M$, for $i = 1$, and $n = N - M + 1,..., N$, for $i = 2$. In this equation a_m^i is the autoregressive process coefficient and ε_n^i refers to the Gaussian distributed noise in the segments, which its mean and variance are $E\{\varepsilon_n^i\} = 0$ and $E\{(\varepsilon_n^i)^2\} = \sigma_i^2$, re-

spectively. The *AR* coefficients in Eq. (1) are used to model the data simultaneously in intervals $[M+1, K]$ and $[K+1, N-M]$. While $K+1$ is the boundary between segments (i.e. the phase arrival). The approximate likelihood function *L* for this modeling procedure is:

$$L(x; K, M, \Theta_1, \Theta_2) = \prod_{i=1}^{2} \left(\frac{1}{2\pi\,\sigma_i^2}\right)^{n_i/2} \exp\left(-\frac{1}{2\sigma_i^2}\left(\sum_{j=p_i}^{q_i}(x_j - \sum_{m=1}^{M} a_m^i x_{j-m})\right)^2\right) \quad (2)$$

where $\Theta_i = \Theta(a_1^i, ..., a_M^i, \sigma_i^2)$ represents the model parameters for interval $p_1 = M+1$, and $q_1 = K$, $q_2 = N-M, n_1 = K-M, n_2 = N-M-K$. The maximum likelihood estimation of the model parameters is found at $\partial \log L / \partial \Theta_i = 0$, with the following solution:

$$\sigma_{i,\max}^2 = \frac{1}{n_i}\sum_{j=p_i}^{q_i}\left(x_j - \sum_{m=1}^{M} a_m^i x_{j-m}\right)^2 \quad (3)$$

The maximum value of the logarithmic likelihood function for both models as a function of *K*, separating point of two intervals, is obtained as:

$$\log(L(x; K, M, \Theta_1, \Theta_2)) = -\frac{1}{2}(K-M)\log(\sigma_{1,\max}^2) - \frac{1}{2}(N-M-K)\log(\sigma_{2,\max}^2) + C \quad (4)$$

where, *C* is a constant. By maximizing the joint likelihood function Eq. (4) as a function of *K*, the best feasible estimate of *K* is calculated. Accordingly, in phase picking problems, x_K is interpreted as the optimal phase onset time.

Eq. (4) is the first term in Akaike's Information Criteria, which is defined as:

$$AIC = -2\log(\textit{maximized likelihood function}) + 2M \quad (5)$$

The first term of Eq. (5) measures the misfit of the *AR* model and the second term, implies the unreliability of the fit [27]. In the phase picking applications, the order of the *AR* model, *M*, considered as a fixed parameter. Therefore, the only variable term of Eq. (5) is the first term. The above described optimization method is referred as *AR-AIC*. Ideally, *AIC* function will linearly decrease from $M+1$ to x_K then increase from x_K+1 to *N-M*. Therefore, it results a "*V*" shape function with the minima at x_K, where x_K is the onset time.

The *AR* coefficients in Eq. (1) are estimated usually by Yule-Walker approach [30], Burge algorithm [31] or the least squares approach. In this paper, we have used a MATLAB function based on the Burge algorithm to calculate *AR* coefficients. The order of an *AR* model can be estimated by partial autocorrelation function (e.g. [30]) or the application of *AIC* [27]. If a small *AR* model order is used in the process, the main statistical properties of the original signal will be ignored; while a big model order causes the modeling of the noise associated with data. Based on [26], we assumed the order of *AR* model to be 4, in this study.

Three different, but fairly similar, approaches have been proposed for phase onset picking based on AR modeling [29]. Figure (1), shows the three approaches which are introduced briefly here. In first approach, Figure (1a), the whole time interval is described by two *AR* models. One model, *F*, is calculated in the interval 1 to *K*-1 and the other one, *B*, is calculated from *K* to *N*. *K* is the division point of two intervals, which is variable and *N* is the length of the segment. In the second approach, Figure (1b), the *F* model, in forwards direction, is calculated on the arbitrary interval 1 to *l* and the *B* model, in backwards direction, is considered on the interval *N*-1 to *N*. Using *F* and *B* model coefficients, the error prediction series on the interval $1+M$ to *N*-*M* and *N*-*M* to $1+M$, are calculated, respectively. The parameter *M* is the model order. After that, using the variance of the prediction error, *AIC* function is calculated at each point. In the third approach, Figure (1c), the *AR* model

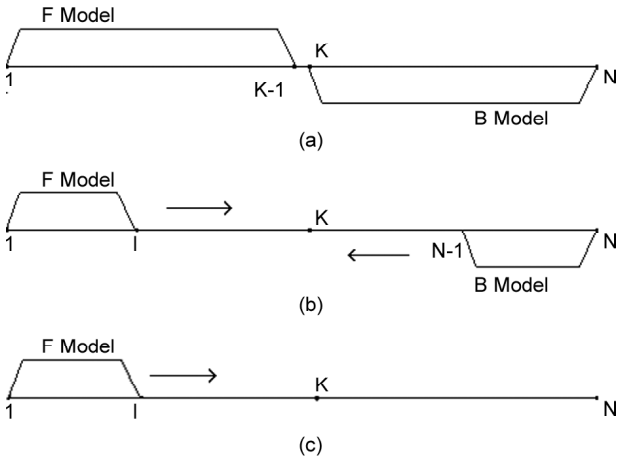

Figure 1. Three approaches used in the AR-based onset time estimation methods, F model refers to forwards model and B model refers to the backwards [29].

(F-model) is obtained once in the first part of the time series. The prediction error series is obtained for the other points. For different K from $1+M$ to $N-M$, the *AIC* function is calculated.

Normally, the *AR* model is applicable only for stationary part of a signal. Accordingly, regarding that the segment which contains the S-wave group is not stationary; the third approach is taken in this paper for S-phase picking.

One approach for S-phase detection based on the *AR* modeling is using the sum of the AIC's of two or three *AR* models obtained by fitting to each component [22]. We have used this approach to make a comparison between the results of the proposed method and *AR* based automatic S-phase picker.

3. Automatic S-Phase Picker and Evaluation

The proposed S-phase picker is based on the time domain 3D covariance matrix eigenvalue analysis and the *AIC* function. The advantage of the proposed method is that the *CF* and the detection rules, are not complicated and do not require many predefined parameters. Therefore, the algorithm can be implemented easily. We emphasis on the idea of using eigenvalue sequences to detect S-phases, as Magotra [32] used to detect S-phase and other secondary waves in an automatic algorithm of single station location. Eigenvalues of covariance matrix give a measure of the localized energy on the direction of the three principal axes of the polarization ellipsoid. In this work, we consider only the biggest eigenvalue sequence, as it is more sensitive to the variation of the seismic signal energy in the direction of wave propagation. While the eigenvectors represent an orthogonal base of the three-dimensional space and form an ellipsoid that best fits to the data in least squares sense [32]. If we assume that earth structure in the vicinity of the receiver is sufficiently homogeneous that no phase shift is introduced by local scattering effect, time domain covariance matrix is calculated via the following equation [33]:

$$C_{3D} = \begin{bmatrix} \sigma_n^2 & \sigma_{ne} & \sigma_{zn} \\ \sigma_{ne} & \sigma_e^2 & \sigma_{ez} \\ \sigma_{zn} & \sigma_{ez} & \sigma_z^2 \end{bmatrix} \quad (6)$$

where:

$$\sigma_n^2 = E[n^2],\ \sigma_e^2 = E[e^2],\ \sigma_z^2 = E[z^2] \quad (7)$$

and,

$$\sigma_{ne} = E[ne],\ \sigma_{zn} = E[zn],\ \sigma_{ez} = E[ez] \quad (8)$$

where, $E[\ ]$ refers to the expected value and n, e and z indicate the north-south, east-west and vertical components. Every element of the covariance matrix reflects the magnitude of the association between two components of the seismogram. Therefore, the corresponding eigenvalues somehow reflect the joint behavior of all three components. For this reason, using the eigenvalue sequence is advantageous over the other energy measurements which regards the total energy of the seismogram as $(n^2 + e^2 + z^2)$ and simply show the envelope of the seismograms. Figure (2) shows an example of seismogram and corresponding total energy (dark line) and eigenvalue sequence (light line). As it is obvious in the lower plot of this figure, eigenvalue sequences are less sensitive to the small amplitude and less correlated background of S waveform in comparison with the S waveform.

The procedure we have proposed is applicable through the following steps:

Step 1) Prefiltering: As a preprocessing of the data, the high-pass Butterworth filter of order 2 is applied on the 3-component seismograms to remove unwanted background noise below 2 Hz.

Step 2) Calculating the characteristic function: The polarization analysis is done on the filtered seismogram using the sliding time windows, which move one sample to the right. In this study, a moving time window of 30 samples (~1/2 second) is considered. It is required that the selected time window be long enough to include the lowest frequency content of the signal. Using the biggest eigenvalue of the 3D covariance matrices a sequence is obtained, which serves as the *CF*, in which a picking algorithm is applied in order to detect the arrival of S-phase waveform. As the P-phase onset time assumed to be known, the *CF* is calculated within a time window, beginning from the P-phase onset time and lasting to the end on the earthquake signal coda, where the S-phase expected to be detected.

Step 3) First estimation of S-phase onset: The *CF* remains small for seismic noise or P-phase which appears before the S-phase group, but increases strongly as S-phase arrives and efficiently tracks the variation of the energy in the 3-component seismogram. The global maximum of the *CF* is mostly

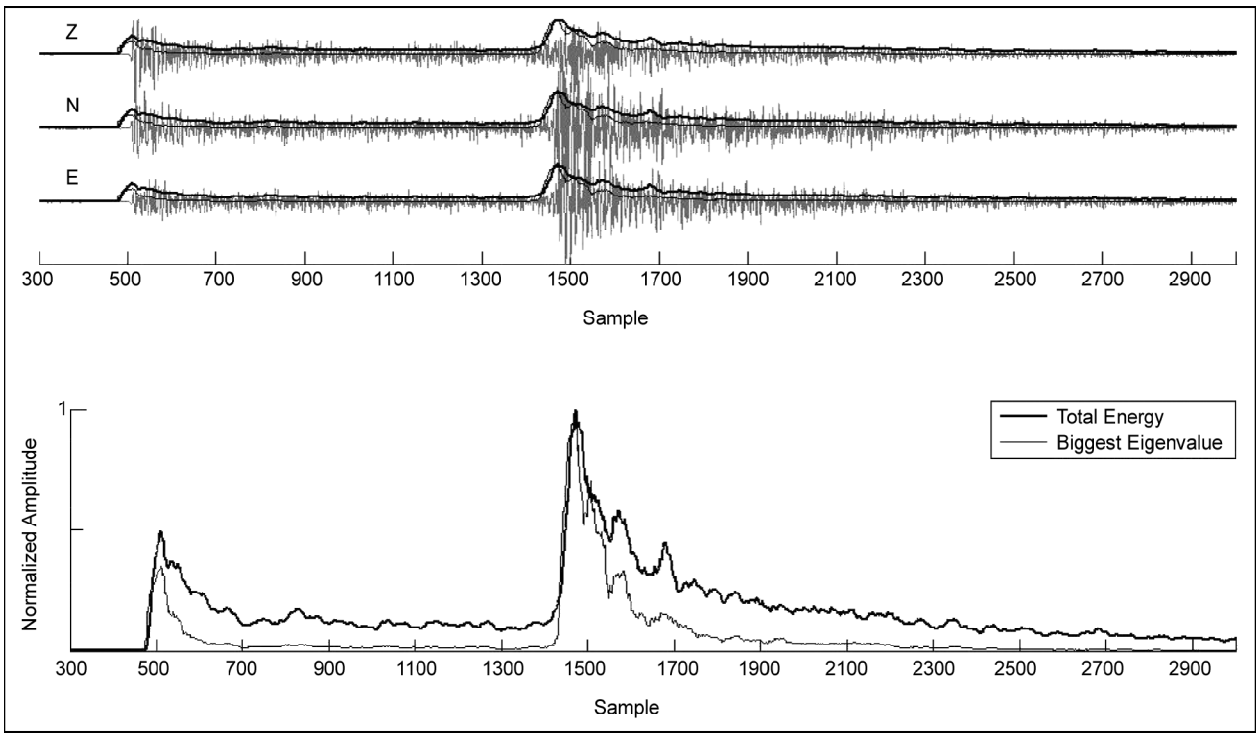

Figure 2. An example of a seismogram (high pass filter, 2 Hz) and corresponding total energy (dark line) and biggest eigenvalue sequence (light line). The total energy time series has been smoothed by averaging in 30 sample time windows. Moving time window of 30 samples are also used in eigenvalue analysis. In the upper plot, both total energy and eigenvalue sequence are normalized to the maximum of the Z component. Sampling interval is 0.02 s.

related to the S-phase waveform. For shallow events, the global maximum of the *CF* may be related to the surface waves. The S-phase onset determination on the *CF* is done using an iterative scheme. The initial estimation of the S-phase onset time is obtained by applying an adaptively selected threshold value on the *CF*. The first point before the global maxima of the *CF* in which the value of the *CF* drops below the threshold value, THR $(=0.15max(CF))$, is regarded as the first estimation of the S-phase arrival time. The coefficient 0.15 is determined experimentally. This value is selected regarding the values of the *CF* in an interval between P-and S-wave group for several signals. While the first estimation of S-phase onset time, $S_{Initial}$, is provided, the algorithm selects 12 seconds of *CF* around it and carries on towards the final S-onset time picking. However, invalid picks are discarded by checking the preliminary phase detection and predicted S-phase arrival time using the earth velocity model. Invalid early picks are usually due to secondary P-phases (e.g. *Pg*), and late picks belongs to the surface waves, which can easily be discriminated from S-phases.

Step 4) Second estimation of S-phase: The AIC function is applied on the selected time window of *CF* to highlight the boundary between S-phase and its background. Accordingly, we obtained the second estimation of S-phase onset time. The *AIC* function originally used to calculate an optimal order for an *AR* model, the criterion can be used to denote the dividing point of two adjacent time series with different underlying statistics. The AIC function can be used for *CFs*, which should not be necessarily defined using *AR* models [26, 34].

$$AIC(K) = (K-1)\log\left(\frac{1}{K}\sum_{j=1}^{K} CF_j^2\right) + (N-K+1)\log\left(\frac{1}{N-K+1}\sum_{j=K}^{N} CF_j^2\right) \quad (9)$$

where, N is the length of the *CF* within the time window. We used above equation to calculate *AIC*, for every assumed K, division point, from the selected time window of the *CF* around first estimation of the S-phase. The S-phase onset time is assigned to the global minimum of the *AIC*-function. The application of above mentioned procedures are shown in following examples.

Figure (3) shows 3-component seismogram of a 3.5 magnitude earthquake, which is recorded in the

GHIR station in local distance (64 km), on 01.01.2005 at 01:31:31. The *CF* is shown at the top of the figure. As it can be seen, the maximum of the *CF*, points to the S-phase group. S-phase onset time, as the operator picked is shown in the figure by a dash line. In this case, the first estimation of the S-phase onset time is 3 samples after the manually picked onset time. The selected time window which is needed for further analysis is shown on the figure as well. Figure (4) shows the *AIC* function (Left) as well as the zoomed version of the analyzing window of *CF* (Right). The global minimum of the *AIC* function refers to the second estimation of the S-phase onset time in the proposed procedure. In this case, the difference ($t_{operator}$- $t_{algorithm}$) of automatically determined S-phase onset and the manual one is 14 samples.

In Figure (5), another example for showing the performance of the proposed algorithm on a local seismogram is shown. The 3-component seismogram belongs to a 3.2 magnitude event recorded in BNDS station on 04.01.2005, at 16:58:59. The epicentral distance is 166 km. In the *CF* time series (left), the global maximum is situated in the S-phase waveform.

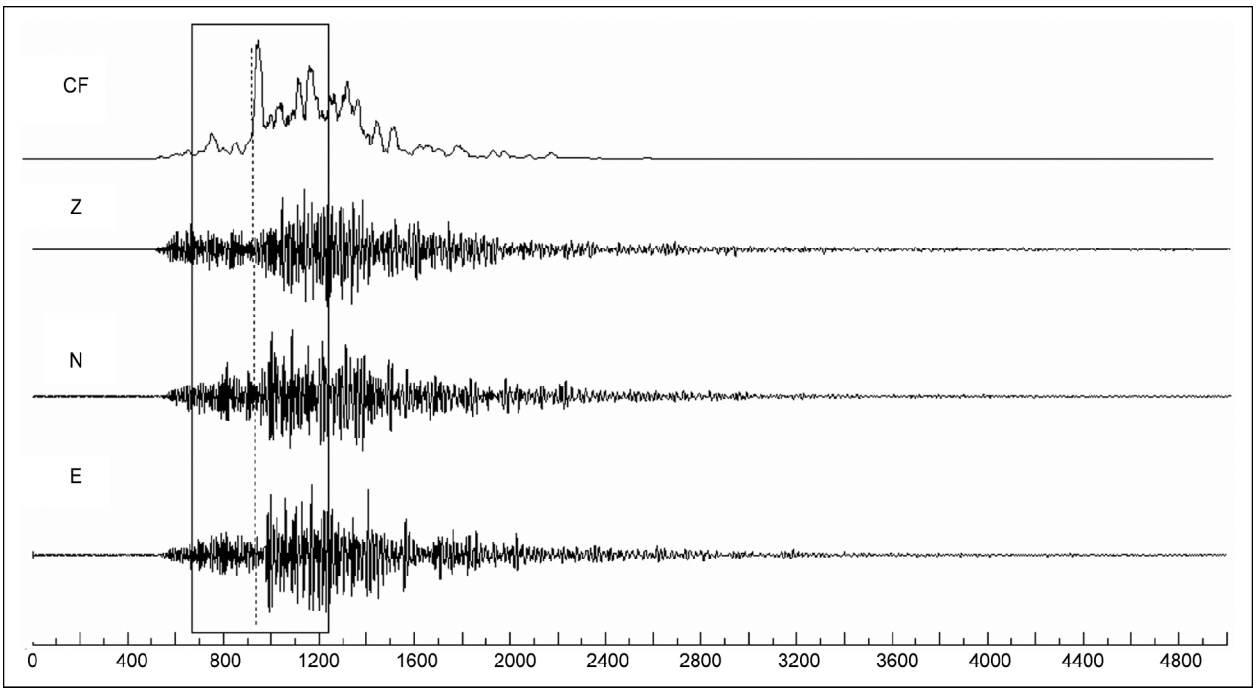

Figure 3. A 3-component seismogram (high pass filter, 2 Hz) of 3.5 magnitude earthquake, recorded in the GHIR station in local distance (64 Km) (case no. 1, Table 1). The horizontal axis shows the number of samples. Sampling interval is 0.02 s. The CF (top) shows abrupt increase in the S-phase waveform. The maximum of the CF belongs to the S-phase waveform. The dash line implies the S-phase onset as determined by the operator. The rectangular on the plot shows the selected window for further analysis. Sampling interval is 0.02 s.

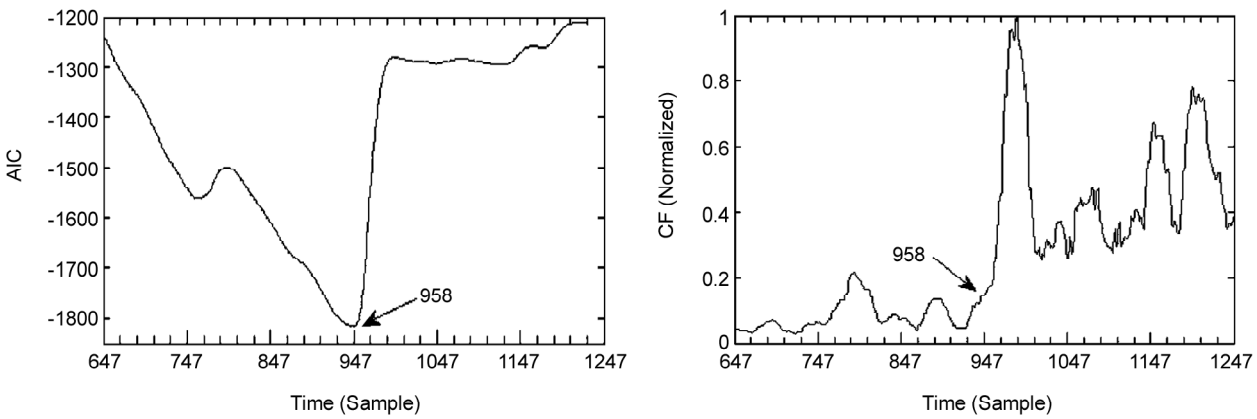

Figure 4. The AIC function (Left), analyzing window of CF (Right). The global minimum of the AIC function refers to the second estimation of the S-phase onset time. Sampling interval is 0.02 s.

The *CF* increases while the S-phase appears on the related seismogram. Figure (6) illustrates the automatic second estimation. To do this, the *AIC* function (Left) and the *CF* around the first estimation of S-phase onset (Right) are shown. The global minimum of the *AIC* indicates the second estimation of S-phase onset. In this case, the differences of the first estimation and second estimation regarding the manual picks are -49.5 and 17.5 samples, respectively.

Figure (7) illustrates another example for a near regional event. The seismogram is recorded by CHTH station, from an earthquake with magnitude of 3.2 in epicentral distance of 210 km, which occurred on 07.05.2006, at 00:48:23. A zoomed version of the CF and AIC function is shown in Figure (8). Figure (9) depicts a stated window around S-phase arrival time for seismogram shown in Figure (7). The manual detection, theoretical arrival time, first and second estimation of S-phase are shown in this figure. In this case, the differences of the first and second estimation regarding the manual picks are -90.5 and -46.5 samples, respectively.

Figure (7) illustrates another example for a near regional event. The seismogram is recorded by CHTH station, from an earthquake with magnitude of 3.2 in epicentral distance of 210 km, which occurred on 07.05.2006, at 00:48:23. A zoomed version of the *CF* and *AIC* function is shown in Figure (8). Figure (9) depicts a stated window around S-phase arrival time for seismogram shown in Figure (7).

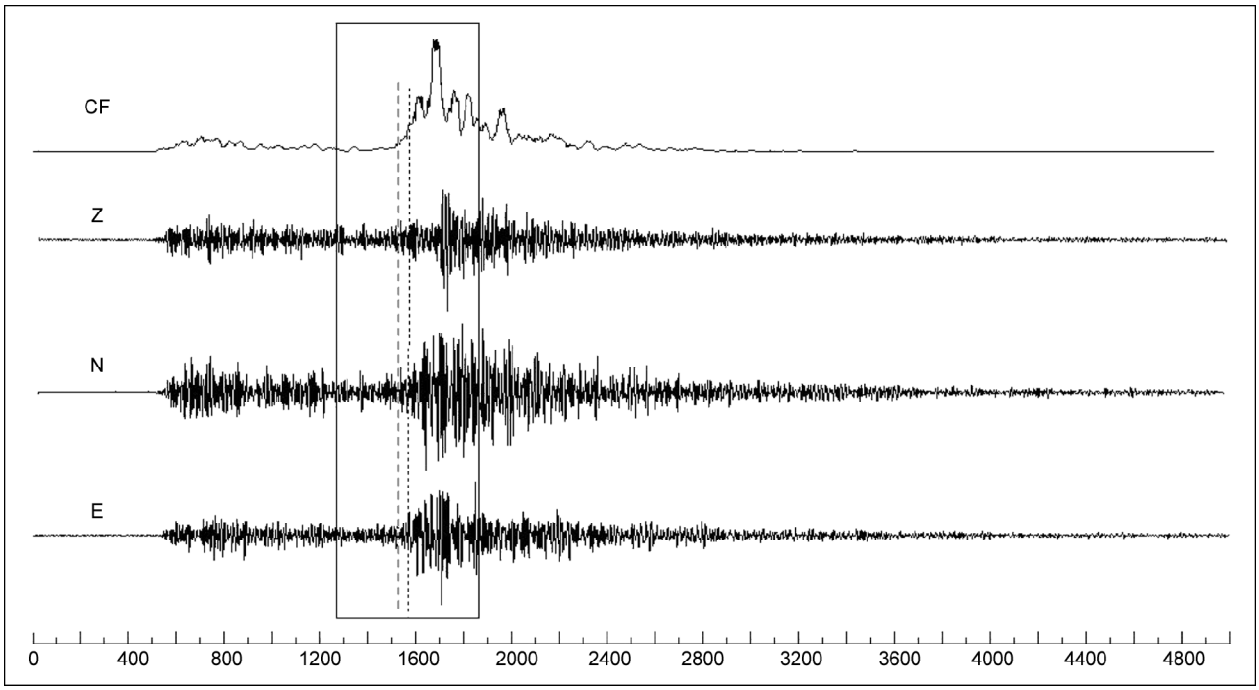

Figure 5. The 3-component seismogram (high pass filter, 2 Hz) of a 3.2 magnitude event, recorded in BNDS station in 2005.01.04, at 16:58:59. The epicentral distance is 166 km (case no. 6, Table (1)). Sampling interval is 0.02 s. In the AIC plot (top), the maximum is situated in S-phase group waveform. The S-phase onset as the operator picked shown by dash line. The dotted line shows the first automatic estimation. The rectangular indicated to the selected window for next step.

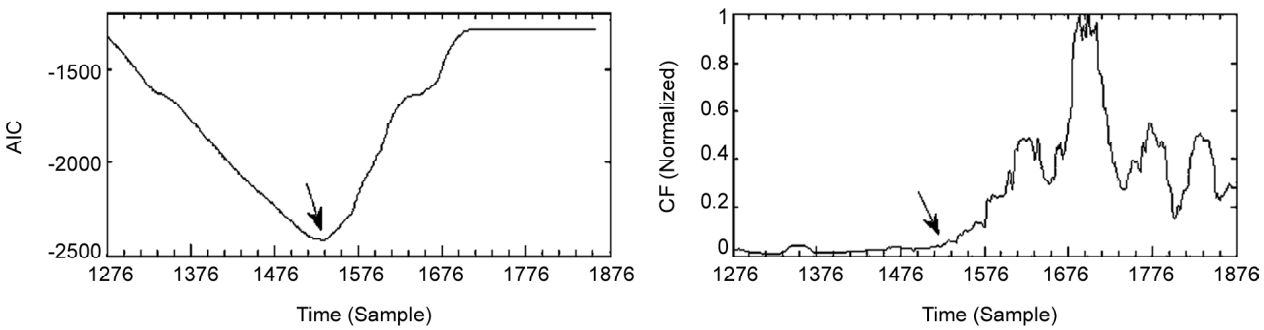

Figure 6. The AIC function (Left) and the CF around the first estimation of S-phase onset (Right) are illustrated. The global minimum of AIC, indicates the second estimation of S-phase onset.

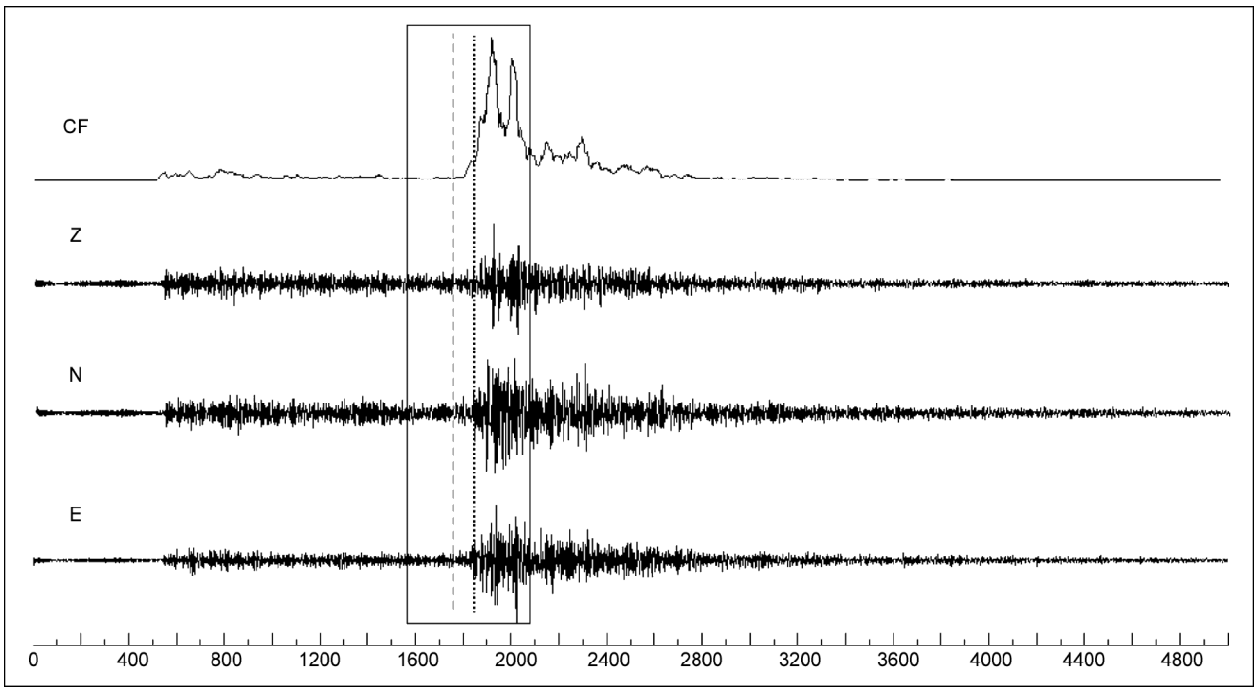

Figure 7. Example of a near regional event (High pass filter, 2 Hz). The seismogram is recorded by CHTH station, from an earthquake with magnitude of 3.2 in epicentral distance of 210 km (case no. 185, Table 1). Sampling interval is 0.02 s. The S-phase onset as the operator picked shown by dash line. The dotted line shows the first automatic estimation. The rectangular indicated to the selected window for next step.

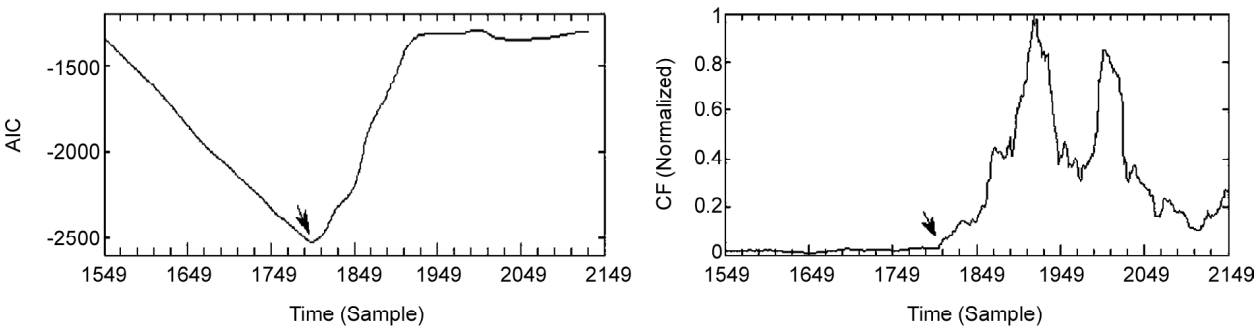

Figure 8. The AIC function (Left) and the CF around the first estimation of S-phase onset (Right) are illustrated. The global minimum of the AIC, indicates the second estimation of the S-phase onset time.

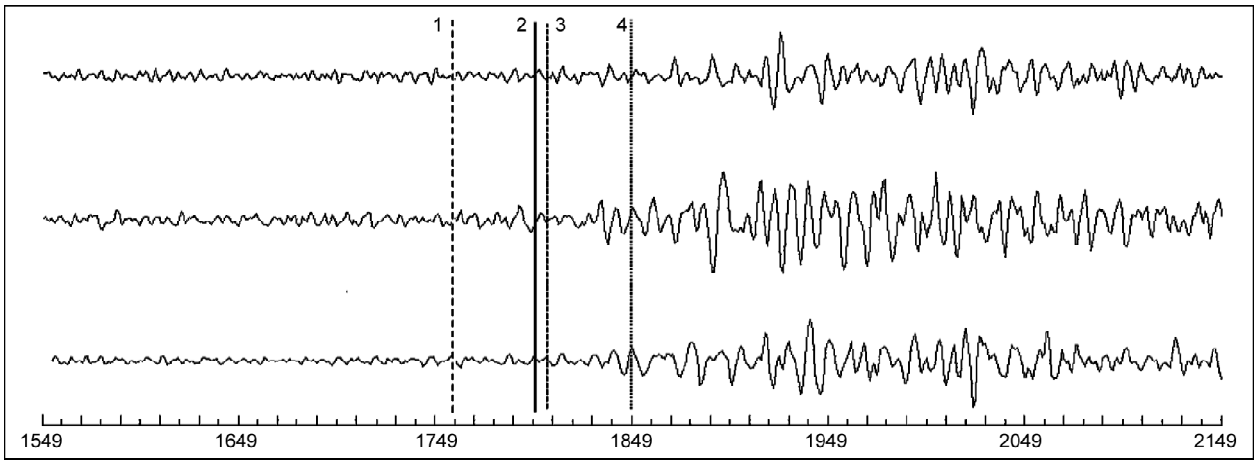

Figure 9. A zoomed window around S-phase arrival time for seismogram shown in Figure (7). The light dash line (no. 1) indicates the manual detection (1758.5), the solid line (no. 2) indicates the second estimation of S-phase (1808), the dark dash line (no. 3) shows the theoretical S-arrival time (1812), and the dotted line (no. 4) shows the first estimation of S-phase (1849) by the automatic procedure.

The manual detection, theoretical arrival time, first and second estimation of S-phase are shown in this figure. In this case, the differences of the first and second estimation regarding the manual picks are -90.5 and -46.5 samples, respectively.

We have examined the performance of the proposed method, by using a database including 185 seismograms selected from BIN data bank. The seismograms are recorded in different broadband stations with 50 samples per second, and belong to the earthquakes most of which have a magnitude range from 2.8 to 3.8 and epicentral distance of about 50 to 300 kilometers. The locations of events and station are shown in Figure (10) and event's magnitude versus receiver to source distance is depicted in Figure (11). The proposed algorithm has been applied on this data set, and S-phase onset times are picked automatically. In order to have insight to accuracy of automatically picked S-phase onset time, a comparison has been done between the automatic picks and manual picks, which are already available for seismograms. We also applied the algorithm on horizontal components, to test whether the results are stable in this case. In addition, we want to know whether using 3-component is essential or not. The results are summarized in Table (1). The second

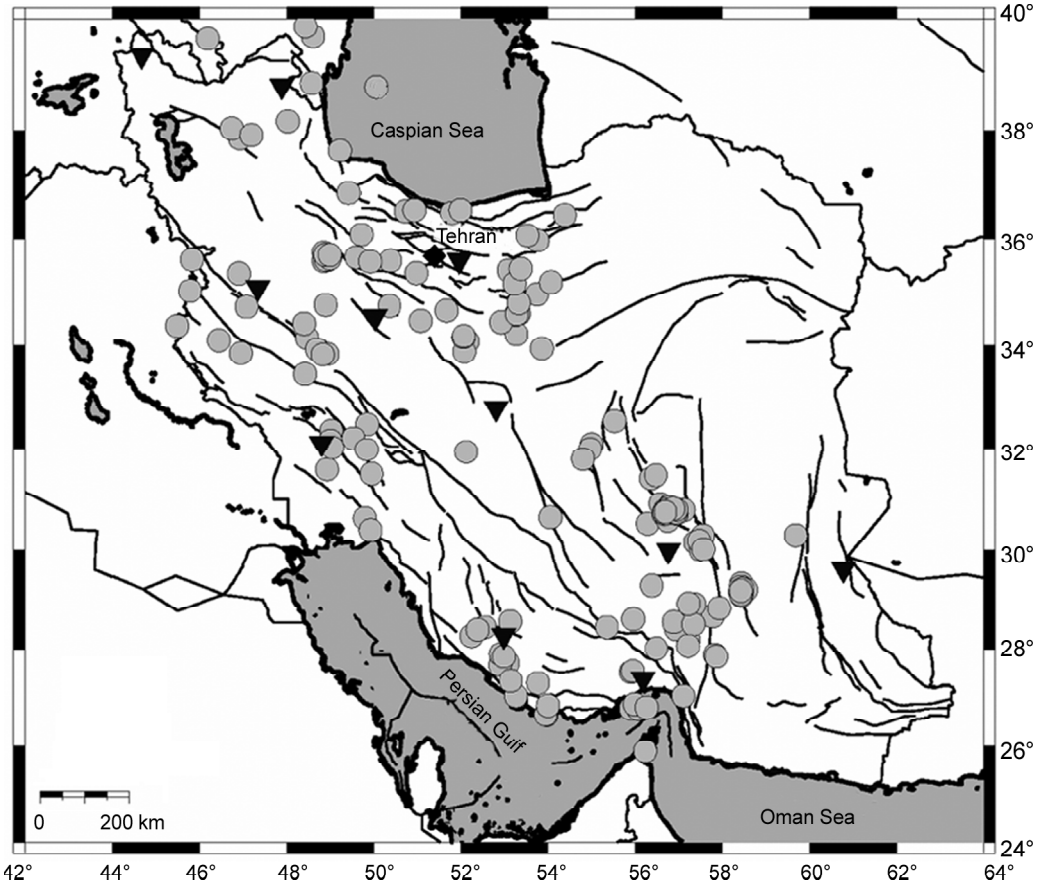

Figure 10. The location map of seismic events (circles) and stations (triangles).

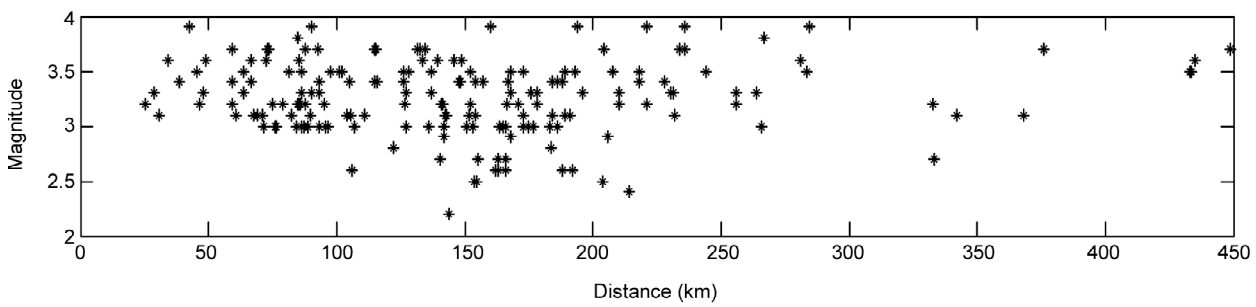

Figure 11. Magnitude of events versus receiver to source distance.

Table 1. Information of database and results of S-phase onset picking.

No.	Displacement	Magnitude	SNR	S-op	$S_{Initial}$	S-AIC-3	S-AIC-2	AR-AIC-3	AR-AIC-2
1	63.71	3.5	39	944	947	958	958	977	977
2	67.5	3.1	83	957	948	954	954	969	969
3	42.55	3.9	67	805	819	815	815	828	828
4	184.2	3.4	54	1591	1616	1586	1586	1621	1621
5	63.47	3.3	60	920	932	935	935	951	972
6	166.7	3.2	32	1526.5	1576	1544	1544	1596	1597
7	153.6	2.5	46	1441	1443	1436	1436	1452	1452
8	84.77	3.8	90	1013.5	1009	1013	1013	1108	1107
9	176.6	3	45	1591	1673	1628	1626	1640	1680
10	71.75	3	61	963.5	964	974	970	1005	1005
11	152.3	3.2	25	1437.5	1510	1470	1457	1568	1568
12	173	3.5	57	1524	1575	1515	1514	1583	1578
13	45.68	3.5	70	845	860	848	849	889	888
14	134.5	3.7	43	1344.5	1351	1331	1338	1357	1345
15	115.4	3.7	96	1186.5	1183	1180	1179	1186	1199
16	48.17	3.3	86	812.5	807	824	824	843	851
17	178.5	3.3	68	1602	1623	1585	1585	1624	1621
18	34.32	3.6	79	791.5	802	811	814	831	831
19	183.9	2.8	26	1626	1625	1614	1614	1631	1631
20	72.55	3.6	45	961	948	941	941	958	958
21	178.3	3.2	54	1618.5	1648	1644	1649	1663	1663
22	256.1	3.2	-12	2122	2150	2135	2131	2173	2169
23	133.6	3.6	11	1321.5	1327	1329	1329	1427	1427
24	150.5	3	48	1438	1461	1455	1454	1470	1474
25	102	3.5	86	1084	1091	1074	1074	1090	1094
26	75.84	3	58	1035	1066	1080	1080	1130	1130
27	86.38	3.5	47	1071.5	1061	1089	1137	1201	1201
28	84.61	3.2	83	1009	1031	1037	1036	1052	1099
29	93.05	3.3	66	1094	1083	1086	1086	1104	1104
30	87.78	3.7	91	1065.5	1157	1072	1072	1195	1195
31	163.4	3	49	1484	1489	1484	1484	1500	1500
32	105.2	3.4	79	1185	1179	1187	1187	1242	1242
33	95.1	3.2	66	1108	1068	1109	1080	1149	1149
34	93.4	3.4	71	1107.5	1073	1142	1141	1156	1173
35	82.48	3.1	81	1046.5	1034	1049	1057	1084	1077
36	433.3	3.5	17	3097.5	3144	3143	3143	3158	3158
37	433.3	3.5	22	3465.5	3512	3511	3511	3526	3526
38	435	3.6	7	3458.5	3563	3511	3513	3582	3660
39	126.4	3.2	55	1264	1248	1240	1232	1263	1263
40	59.2	3.7	96	886	878	866	867	886	882
41	265.9	3	4	2221	2255	2256	2251	2271	2288
42	234	3.7	30	1880.5	2079	1921	1921	2338	2308
43	204.1	3.7	17	1738	1766	1768	1768	1783	1786
44	90.44	3.9	84	1086.5	1074	1079	1079	1095	1094
45	122.3	2.8	60	1277.5	1337	1301	1299	1349	1353
46	432.9	3.5	19	3451.5	3544	3501	3551	3569	3565
47	137.1	3.5	43	1348	1397	1384	1387	1403	1402
48	332.8	3.2	26	2702	2693	2700	2694	2712	2712
49	235.6	3.9	34	1895	1864	1881	1882	1998	2004
50	86.48	3	49	1063.5	1042	1046	1044	1071	1071
51	141.4	3.2	67	1394.5	1387	1389	1385	1443	1443
52	46.61	3.2	100	846.5	861	858	858	876	877
53	147.6	3.4	69	1438	1478	1477	1479	1493	1492
54	89.51	3.1	68	1049.5	1033	1034	1034	1052	1052
55	97.79	3.5	86	1102.5	1104	1105	1104	1120	1138
56	152.3	3.5	59	1431	1456	1441	1440	1460	1460
57	244.4	3.5	37	1985	2005	1998	1998	2011	2011
58	266.7	3.8	56	2167	2167	2152	2151	2166	2187
59	144	2.2	35	1393.5	1417	1379	1379	1417	1417
60	139.3	3.6	83	1379	1537	1372	1370	1423	1816
61	87.41	3	72	1066.5	1084	1094	1096	1113	1113
62	140.4	2.7	44	1377	1408	1390	1389	1410	1423
63	96.68	3	43	1060	1056	1058	1058	1073	1073
64	71.1	3.1	87	967	960	962	961	976	976
65	95.75	3	102	1081.5	1077	1073	1073	1086	1086
66	66.53	3.4	86	945.5	948	949	949	968	968
67	368.3	3.1	-16	2957.5	3041	2971	3047	3057	3072
68	87.9	3.2	64	1074	1064	1069	1066	1085	1085
69	85.16	3.6	77	1064.5	1075	1078	1078	1094	1094
70	81.55	3.5	68	1055.5	1065	1066	1064	1082	1082

Table 1. Continue...

No.	Displacement	Magnitude	SNR	S-op	$S_{Initial}$	S-AIC-3	S-AIC-2	AR-AIC-3	AR-AIC-2
71	214.2	2.4	4	1774.5	1800	1800	1805	1816	1813
72	59.08	3.2	55	904.5	906	906	905	920	925
73	86.05	3.2	81	1070	1106	1062	1062	1150	1159
74	175.8	3.3	50	1532	1522	1519	1519	1538	1538
75	154.8	2.5	43	1454.5	1507	1496	1511	1529	1526
76	142.1	3	31	1379	1418	1422	1422	1477	1499
77	105.4	3.1	43	1151	1189	1194	1193	1222	1224
78	132.6	3.7	73	1338	1338	1337	1337	1353	1353
79	448.9	3.7	17	3612	3758	3642	3660	3784	3779
80	59.17	3.4	77	884.5	887	885	885	904	898
81	107	3	43	1209.5	1249	1241	1229	1266	1266
82	114.7	3.7	84	1245	1251	1256	1251	1272	1272
83	154.1	3.1	58	1446.5	1482	1477	1477	1495	1494
84	230.2	3.3	32	1895.5	1895	1901	1892	2032	2041
85	72.83	3.7	108	957	943	946	946	965	965
86	151.9	3.1	7	1441.5	1433	1427	1427	1444	1447
87	110.7	3.1	72	1179	1164	1160	1160	1176	1179
88	231.8	3.1	29	1904	1944	1942	1942	1961	1961
89	283.4	3.5	23	2338.5	2360	2361	2360	2380	2380
90	142.3	3.1	43	1359.5	1371	1376	1376	1440	1440
91	131.6	3.7	67	1332.5	1330	1325	1325	1339	1339
92	231.6	3.3	19	1878.5	1905	1908	1906	1919	2038
93	153	3	49	1462	1444	1443	1443	1472	1476
94	85.4	3.2	67	1050.5	1073	1076	1077	1134	1094
95	143	3.1	60	1388	1402	1399	1398	1462	1445
96	142	2.9	42	1390.5	1422	1405	1404	1436	1443
97	38.8	3.4	112	767.5	759	760	759	776	776
98	115	3.4	76	1218	1221	1213	1210	1224	1229
99	186	3.4	56	1640	1695	1624	1624	1641	1647
100	136	3	54	1408.5	1440	1412	1409	1455	1455
101	165	3	39	1497	1490	1519	1519	1539	1600
102	266	3	2	2335.5	2356	2343	2362	2382	2377
103	183	3	56	1712.5	1724	1709	1709	1725	1725
104	168	2.9	82	1521.5	1525	1522	1522	1538	1538
105	167	3.4	86	1501	1524	1521	1520	1540	1540
106	106	2.6	42	1171.5	1169	1186	1171	1222	1222
107	281	3.6	17	2349	2496	2379	2547	2566	2567
108	25.3	3.2	49	703.5	743	733	719	733	750
109	256	3.3	42	2020	2130	2063	2063	2182	2151
110	189	3.5	11	1636	1642	1645	1645	1663	1663
111	90.3	3.3	59	1069.5	1054	1066	1066	1084	1084
112	221	3.2	49	1875	1901	1891	1892	1911	1910
113	136	3	32	1353.5	1406	1393	1393	1410	1411
114	75.1	3.2	63	982.5	1090	1020	1019	1155	1155
115	221	3.9	43	1868	1894	1889	1889	1938	1907
116	166	3	33	1525	1538	1543	1543	1633	1622
117	141	3.2	47	1341	1405	1383	1383	1426	1426
118	84.5	3	66	1089.5	1085	1087	1087	1134	1104
119	86.4	3.3	84	1043.5	1032	1064	1064	1157	1155
120	128	3.5	38	1292.5	1458	1285	1276	1479	1479
121	189	3.1	41	1608.5	1643	1643	1641	1656	1656
122	92.9	3.7	70	1111.5	1087	1114	1114	1230	1231
123	218	3.4	43	1873.5	1942	1884	1886	1957	1957
124	163	2.7	18	1511.5	1514	1512	1509	1526	1529
125	166	2.7	30	1522	1519	1518	1518	1533	1533
126	116	3.4	33	1228	1277	1273	1269	1288	1288
127	160	3.9	67	1500.5	1531	1518	1514	1534	1538
128	157	3.4	25	1465.5	1463	1465	1479	1488	1483
129	146	3.6	98	1389	1441	1432	1431	1461	1461
130	196	3.3	51	1708	1711	1706	1705	1722	1723
131	193	3.5	66	1676.5	1712	1702	1702	1719	1720
132	204	2.5	-4	1724.5	1707	1708	1704	1752	1753
133	191	3.1	44	1659.5	1700	1676	1669	1687	1700
134	192	2.6	6	1660.5	1713	1666	1665	1721	1721
135	163	2.6	63	1509	1528	1511	1511	1531	1541
136	166	2.6	34	1504	1517	1499	1499	1518	1514
137	162	2.6	49	1473.5	1521	1508	1508	1526	1526
138	186	3	80	1614	1608	1604	1604	1621	1621
139	188	2.6	17	1614.5	1629	1619	1619	1638	1639
140	168	3.5	56	1528	1548	1548	1548	1582	1582

Table 1. Continue...

No.	Displacement	Magnitude	SNR	S-op	$S_{Initial}$	S-AIC-3	S-AIC-2	AR-AIC-3	AR-AIC-2
141	93.1	3	77	1102	1063	1112	1080	1126	1132
142	126	3.5	88	1293.5	1275	1302	1302	1320	1322
143	184	3.1	39	1620.5	1610	1608	1608	1625	1625
144	168	3.3	80	1516.5	1516	1510	1510	1529	1524
145	333	2.7	94	2688	2774	2691	2687	2806	2795
146	264	3.3	54	2169.5	2271	2210	2110	2394	2406
147	171	3.2	81	1557.5	1589	1570	1564	1596	1615
148	210	3.3	56	1785	1810	1807	1806	1820	1821
149	188	3.4	95	1643.5	1745	1686	1755	1774	1774
150	73.4	3.7	12	988.5	962	966	967	985	1068
151	69.3	3.1	36	957	944	952	948	981	981
152	206	2.9	53	1764.5	1758	1746	1745	1763	1763
153	88.6	3	33	1092.5	1088	1084	1083	1101	1102
154	155	2.7	40	1430.5	1452	1439	1451	1470	1467
155	149	3.6	47	1455.5	1442	1443	1441	1500	1500
156	154	3.4	41	1449	1440	1432	1428	1446	1446
157	228	3.4	48	1884.5	1875	1860	1848	1886	1882
158	127	3	36	1350	1356	1350	1348	1359	1359
159	284.7	3.9	3	3048.5	3064	3054	3055	3074	3074
160	136	3	28	1353.5	1381	1353	1352	1370	1371
161	34.4	3.6	73	780	832	787	787	806	806
162	208	3.5	31	1762	1793	1771	1767	1813	1813
163	48.9	3.6	107	821.5	802	830	811	842	842
164	78.9	3.2	77	1006.5	998	997	997	1013	1013
165	218	3.5	6	1798.5	1760	1766	1763	1816	1824
166	126	3.4	32	1280.5	1289	1287	1285	1304	1304
167	60.57	3.1	20	897	976	899	898	1015	996
168	148.1	3.4	52	1425	1515	1440	1426	1537	1614
169	375.8	3.7	7	3054.5	3030	3077	3065	3095	3095
170	173	3	55	1536	1595	1553	1551	1604	1587
171	194	3.9	42	1684.5	1679	1678	1681	1692	1691
172	66.83	3.6	36	943.5	940	943	941	974	978
173	85.3	3.2	45	1067.5	1060	1066	1066	1140	1140
174	76.6	3	29	1007.5	991	993	991	1005	1008
175	127	3.3	22	1286	1315	1302	1301	1315	1329
176	236	3.7	51	1890.5	1872	1874	1873	1895	1899
177	104	3.1	40	1125.5	1087	1101	1089	1135	1206
178	30.9	3.1	74	741.5	735	728	728	746	747
179	28.6	3.3	80	732	766	731	730	746	782
180	137	3.3	53	1312.5	1396	1316	1315	1524	1536
181	175	3	45	1539.5	1530	1526	1526	1544	1544
182	101	3.5	32	1169	1173	1178	1175	1193	1193
183	173	3.1	50	1562	1589	1574	1572	1590	1591
184	342	3.1	2	2788	2808	2806	2806	2829	2830
185	210	3.2	22	1758.5	1849	1808	1974	1808	1974

column of the table shows the epicentral distance of every event while the third column includes its local magnitude. The signal to noise ratio (SNR) of P-phase waveform is shown in fourth column. The columns 5 to 7 show the S-phase onset sample as the operator is picked (S-op), the first estimation of S-phase ($S_{Initial}$) and the second estimation of S-phase onset time by the proposed algorithm (S-*AIC*-3), respectively. The eighth column shows the S-phase onset time as determined using horizontal components (S-*AIC*-2).

Time difference between the manual S-phase onset time and automatically detected ones are shown in the Figure (12), for both first and second estimation of S-phase onset obtained from proposed algorithm.

In order to show the advantage of using *AIC* function using presented *CF* over the *AR-AIC* method and to see how the proposed method performs in comparison with the *AR-AIC* method, we also examined the database using *AR-AIC* on 3-component as well as 2-component seismogram. The analysis is done in the selected time window around the first estimation of the S-phase. As an example, the AR-AIC functions for seismogram previously shown on Figure (3) are illustrated in Figure (13). Results obtained for our database are shown in ninth column of Table (1) for *AR-AIC* method using 3-component seismogram, see Figure (14), and in tenth column for *AR-AIC* method by

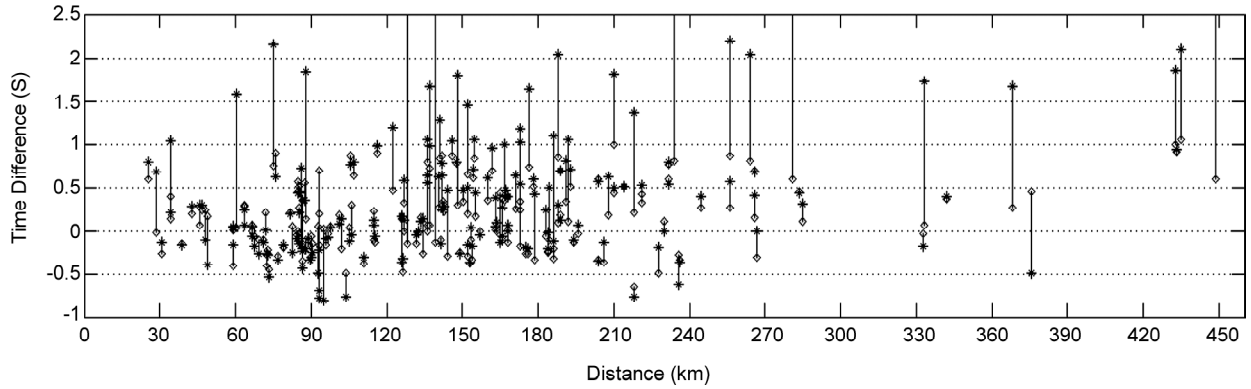

Figure 12. Time differences between manually and automatically detected S-phase for first (stars) and second (open diamonds) estimations for the receiver to source distances of the events.

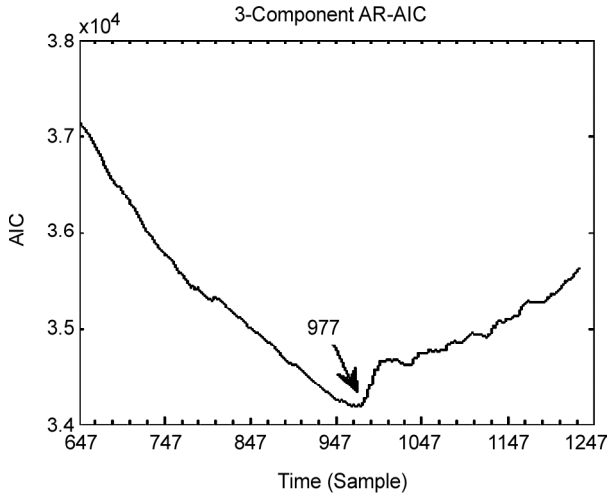

Figure 13. The AIC function obtained for the seismogram shown in the Figure (3) by means of 3-component, global minimum refers to the S-phase onset.

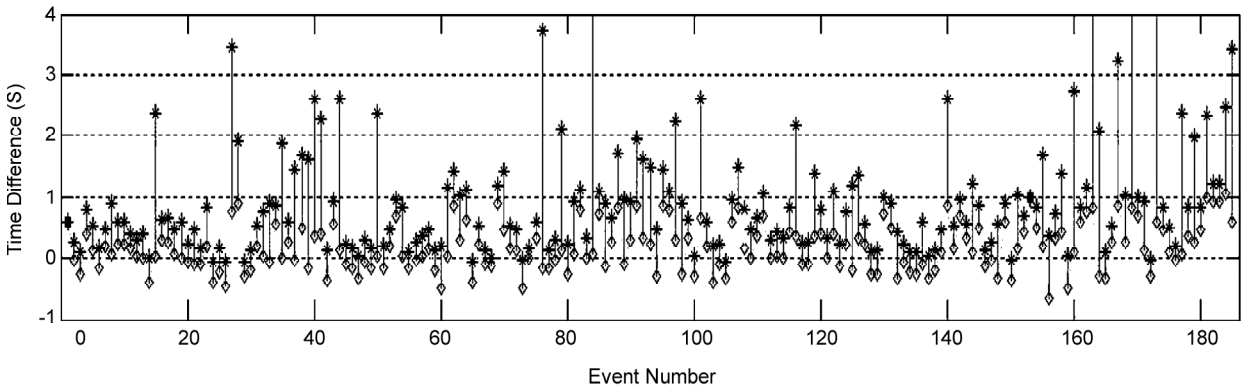

Figure 14. Time differences between manually and automatically detected S-phase for AR-AIC3 (stars) and S-AIC3 (open diamonds).

using just horizontal components.

To have a convenient comparison of the results obtained from different algorithms, the schematic pie diagrams are prepared as Figure (15). As it can be seen, the overall results obtained from second estimation of the proposed method are better than the other methods, even using 2-component seismogram. However, the best results are achieved using 3-componet seismogram. The results obtained from the AR-AIC method for 3-component seismograms are the same as 2-component seismograms with a few differences of a 1-3 % in every sector.

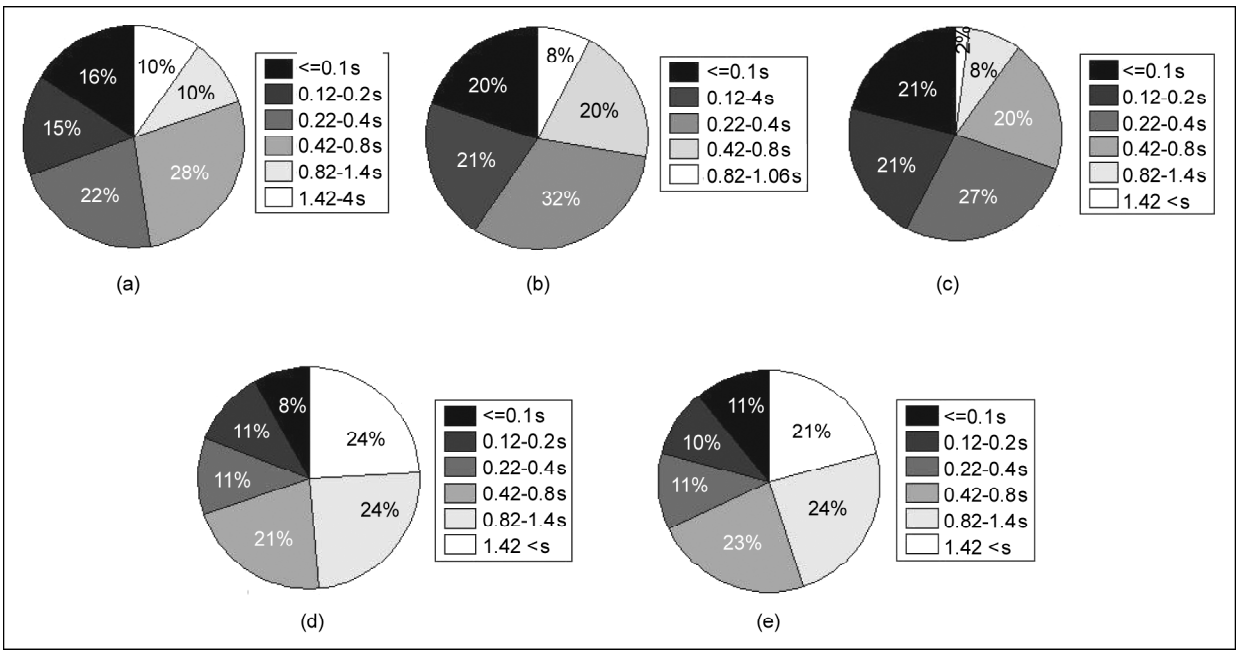

Figure 15. Pie diagrams for comparing results of different algorithms on our database. The percentages of absolute number of sample difference of automatically picked S-phase with manual ones are shown for each algorithm. (a) Results of first estimation, $S_{Initial}$. (b) Results of the second estimation from the proposed method. (c) Results of second estimation of the proposed method by using horizontal components. (d) Results of AR-AIC using 3-Component, (e) Results of AR-AIC using horizontal component.

4. Conclusions

In this paper, an automatic method for S-phase picking in local and near regional distances is presented. The advantage of this method is using a *CF* defined as eigenvalues of a 3D covariance matrix. The *CF* simply tracks the variation of the localized energy of the seismogram. In every window, the value of the *CF* is related somehow on the total energy of the seismogram. However, this is not a true measure of the seismogram energy. This method is also applicable for 2D covariance matrix. As shown in Table (1), the mean value and standard deviation of the automatic S-phase onset deviation from manual ones are -8 and 18 samples, respectively, for second estimation of S-phase onset picking using 3-component analysis. The automatic S-phase onset times determined by the proposed method are compared with those obtained by means of AR-AIC algorithm on 3-component and 2-component seismograms. The overall comparison shows that the proposed method produces more accurate picks which looks like the manual picking. We have investigated the deviations in results, and found that, in some cases, the deviation is due to the high-pass filter attribute. Therefore, if filtering is done based on epicentral distance range, then results may show least deviations.

It should be noted that the deviation from manual picks do not always imply the automatic false picks. Due to the complexity of the S-phase waveform, even manual reading may not always be reliable and robust. In some cases, they are picked at the early beginning point of S-phase waveform while for some cases they are picked more lately. These points indicate unsustainable approach of manual S-phase picking. However, the automatic method works robustly and constantly on the same kind of seismograms.

Acknowledgement

This study is part of a Ph.D. program funded by the International Institute of Earthquake Engineering and Seismology (IIEES) to the first author. We thank Dr. A. Ansary, the head of BIN at IIEES, for providing the necessary data and facilities to do the research. We also thank the critical comments of the reviewers that greatly improved this work.

References

1. Johnson, C.E., Bittenbinder, A., Bogaert, B., Dietz, L., and Kohler, W. (1995). Earthworm: A Flexible Approach to Seismic Network Processing, IRIS Newsletter, **14**, 1-4.

2. Allen, R.V. (1978). Automatic Earthquake Recognition and Timing from Single Traces, Bull. Seism. Soc. Am., **72**, S225-S242.

3. Baer, M. and Kradolfer, U. (1978). An Automatic Phase Picker for Local and Teleseismic Events, Bull. Seism. Soc. Am., **77**, 1437-1445.

4. Withers, M., Aster, R., Young, C., Beiriger, J., Harris, M., Moore, S., and Trujillo, J. (1998). A Comparison of Select Trigger Algorithms for Automated Global Seismic Phase and Event Detection, Bull. Seism. Soc. Am., **88**(1), 95-106.

5. Earle, P.S. and Shearer, P.M. (1994). Characterization of Global Seismograms Using an Automatic-Picking Algorithm, Bull. Seism. Soc. Am., **84**(2), 366-376, 1994.

6. Oonincx, P.J. (1999). A Wavelet Method for Detecting S-Waves in Seismic Data, Computational Geosciences, **3**(2), 111-134.

7. Zao, Y. and Takano, K. (1999). An Artificial Neural Network Approach for Broadband Seismic Phase Picking, Bull. Seism. Soc. Am., **77**(89), 670-680.

8. Chu, C.K. and Mendel, J. (1994). First Break Refraction Event Picking Using Fuzzy Logic Systems, *IEEE Trans. Fuzzy Syst.*, **2**(4), 255-266.

9. Thurber, C.H. and Atre, S.R., (1993). Three-Dimensional VP/VS Variations Along the Loma Prieta Rupture Zone, Bull. seism. Soc. Am., **83**(3), 717-736.

10. Lay, Th. and Wallace, T.C. (1995). Modern Global Seismology, Academic Press, California.

11. Summery of the Bulletin of the International Seismological Center (2008). www.isc.ac.uk/.

12. Gomberg, J.S., Shedlock, M.K., and Roecker, S.W. (1990). The Effect of S-Wave Arrival Times on the Accuracy of Hypocentrer Estimation, Bull. Seism. Soc. Am., **80**(6), 1605-1628.

13. Sadeghi, A., Fatemi Aghda, S.M., Suzuki, S., and Nakamura, T. (2006). 3-D Velocity Structure of the 2003 Bam Earthquake Area (SE Iran): Existence of a Low-Poisson's Ratio Layer and Its Relation to Heavy Damage, *Tectonophysics*, **417**, 269-283

14. Ozel, O., Iwasaki, T., Moriya, T., Sakai, S., Maeda, T., Piao, C., Yoshii, T., Tsukada, S., Ito, A., Suzuki, M., Yamazaki, A., and Miyamachi, H. (1999). Crustal Structure of Central Japan and Its Petrological Implications, *Geophysical Journal International*, **138**, 257-274.

15. Karamzadeh, N., Javan, Gh.D., and Reza Ali. M. (2012). Automatic Earthquake Signal Onset Picking Based on the Continuous Wavelet Transform, Accepted in IEEE Transactions on Geoscience and Remote Sensing, doi: 10.1109/TGRS.2012.2213824.

16. Aki, K. and Richards, P. (1980). Quantitative Seismology, W.H. Freeman, New York.

17. Cichowicz, A. (1993). An Automatic S-Phase Picker, Bull. seism. Soc. Am., **83**(1), 180-189.

18. Roberts, R.G. and Christoffersson A. (1990). Decomposition of Complex Single-Station Three-Component Seismograms, *Geophysical Journal International*, **103**, 55-74.

19. Jepsen, D.C. and Kennett, B.L.N. (1990). Three-Component Analysis of Regional Seismograms, Bull. Seism. Soc. Am., **80**, 2032-2052.

20. Samson, J. and Olson, J. (1980). Some Comments on the Descriptions of the Polarization States of Waves, *Geophys. J. Roy. Astr. Soc.*, **61**, 115-129.

21. Tong, C. and Kennett, B.L.N. (1996). Automatic Seismic Event Recognition and Later Phase Identification for Broadband Seismograms, Bull. Seism. Soc. Am., **86**, 1896-1909.

22. Sleeman, R. and Eck T.V. (2002). Single Station Real-Time P and S Phase Pickers for Seismic Observatories, Methods and Applications of Signal Processing, Springer-Verlag, Berlin.

23. Anant, S.K. and Dowla, F.U. (1997). Wavelet Transform Methods for Phase Identification in Three-Component Seismogram, Bull. Seism. Soc. Am., **87**, 1598-1612.

24. Takanami, T. and Kitagawa, G. (1993). Multivariate Time-Series Model to Estimate the Arrival Times of S-Waves, *Comput. Geosci.*, **192**, 295-301.

25. Takanami, T. and Kitagawa, G. (1991). Estima-

tion of the Arrival Times of Seismic Waves by Multivariate Time Series Model, *Ann. Inst. Stat. Math.*, **43**, 407-433.

26. Kuperkoch, L., Meier, T., Brustle A., Lee J., Friderich W., Egelados Working Group (2011). Automated Determination of S-phase Arrival Times Using Autoregressive Prediction: Application to Local and Regional Distances, *Geophysical Journal International*, **188**(2), 687-702.

27. Akaike, H. (1971). Autoregressive Model Fitting for Control, *Ann. Inst. Statist. Math.*, **23**, 163-180.

28. Leonard, M. and Kennett, B.L.N. (1999). Multi-Component Autoregressive Techniques for the Analysis of Seismograms, *Phys. Earth Planet. Inter.*, **113**, 247-263.

29. Leonard, M. (2003). Application of Autoregressive Processing to the Analysis of Seismograms, Methods and Applications of Signal Processing in Seismic Network Operations, 61-78.

30. Box, G.E.P., Jekins, G.M., and Reinsel, G.C. (1994). Time Series Analysis-Forecasting and Control, Prentice-Hall.

31. Burg, J.P. (1975). Maximum Entropy Spectral Analysis, Ph.D. Thesis, Department of Geophysics, Stanford University.

32. Magotra, N., Ahmed N., and Chael, E. (1989). Single-Station Seismic Event Detection and Location, IEEE Transactions on Geoscience and Remote Sensing, **27**, 15-23.

33. Magotra, N., Ahmed, N., and Chael, E. (1987). Seismic Event Detection and Source Location Using Single-Station (Three-Component) Data, Bull. Seism. Soc. Am., **77**, 958-971.

34. Ahmed, A., Sharma, M.L., and Sharma., A. (2007). Wavelet Based Automatic Phase Picking Algorithm for 3-Component Broadband Seismological Data, *Journal of Seismology and Earthqukae Engineerign (JSEE)*, **9**(1,2), 15-24.